HHS Public Access

Author manuscript

NMR Biomed. Author manuscript; available in PMC 2021 March 19.

Published in final edited form as:

NMR Biomed. 2009 May ; 22(4): 391–404. doi:10.1002/nbm.1348.

A model for the analysis of competitive relaxation effects of manganese and iron *in vivo*

Na Zhang[a,b], **Vanessa A. Fitsanakis**[c], **Keith M. Erikson**[d], **Michael Aschner**[e,f], **Malcolm J. Avison**[a,f,g,h], **John C. Gore**[a,b,g,i,j,*]

[a]Vanderbilt University Institute of Imaging Science, Vanderbilt University, Nashville, Tennessee, USA

[b]Department of Physics & Astronomy, Vanderbilt University, Nashville, Tennessee, USA

[c]Department of Biology, King College, Bristol, Tennessee, USA

[d]Department of Nutrition, University of North Carolina at Greensboro, Greensboro, North Carolina

[e]Department of Pediatrics, Vanderbilt University, Nashville, Tennessee, USA

[f]Department of Pharmacology, Vanderbilt University, Nashville, Tennessee, USA

[g]Department of Radiology & Radiological Sciences, Vanderbilt University, Nashville, Tennessee, USA

[h]Department of Neurology, Vanderbilt University, Nashville, Tennessee, USA

[i]Department of Biomedical Engineering, Vanderbilt University, Nashville, Tennessee, USA

[j]Department of Molecular Physiology and Biophysics, Vanderbilt University, Nashville, Tennessee, USA

Abstract

Manganese (Mn) and iron (Fe) are both paramagnetic species that can affect magnetic resonance relaxation rates. They also share common transport systems *in vivo* and thus in experimental models of metal exposure their effects on relaxation rates may interact in a complex fashion. Here we present a novel model to interpret the combined effects of Mn and Fe on MRI relaxation rates. To achieve varying levels of both metals, adult rats were separated into four groups; a control group and three groups treated with weekly intravenous injections of 3 mg Mn/kg body for 14 weeks. The three treated groups were fed either a normal diet, Fe deficient or Fe enriched diet. All rats were scanned using MRI at the 14th week to measure regional water relaxation rates. Rat brains were removed at the end of the study (14th week) and dissected into regions for measurement of Mn and Fe by atomic absorption spectroscopy. For the normal diet groups, R_1 was strongly correlated with tissue Mn concentrations. However, the slopes of the linear regression fits varied significantly among different brain regions, and a simple linear model failed to explain the changes in relaxation rate when both Mn and Fe contents changed. We propose a competition model, which is based on the ability of Mn and Fe to compete *in vivo* for common binding sites.

*Correspondence to: J. C. Gore, Vanderbilt University Institute of Imaging Science 3rd Floor, VUIIS Building, Medical Center North 1161 21st Ave, South Nashville, TN 37232-2310, USA. john.gore@vanderbilt.edu.

The combined effect of Mn and Fe on the relaxation rates is complicated and additional studies will be necessary to explain how MRI signals are affected when the levels of both metals are varied.

Keywords

manganese; irony; rat brain; MRI; relaxivity; T_1; T_2; model

INTRODUCTION

Magnetic resonance imaging (MRI) is a non-invasive diagnostic imaging technique with potential applications for measuring and monitoring the effects of metal exposure and neurotoxicity. MR images are sensitive to the presence of paramagnetic ions, which increase the relaxation rates of tissue water protons and, in principle, measurements of tissue relaxation rates may be used to monitor tissue metal levels quantitatively. Divalent manganese (Mn) and iron (Fe) ions (Mn^{2+} and Fe^{2+}), and trivalent Fe ion (Fe^{3+}), contain unpaired electrons and are consequently highly effective as paramagnetic relaxation agents capable of shortening both the T_1 and T_2 relaxation times of water molecules (1–5).

Mn and Fe are both essential metals for metabolism and biochemical functions in the central nervous system. Mn is an essential nutrient found in many foods, and is required for proper growth and development. It is an important component of many key enzymes involved in the detoxification of reactive oxygen species, amino acid synthesis and energy production (6,7). Both deficiency and excess of this metal may result in health problems, although Mn toxicity is more common. Too little dietary Mn can lead to growth retardation, alterations in glucose and high-density lipoprotein (HDL) levels and even reproductive failure (8). On the other hand, excess Mn can lead to the onset of a movement disorder, termed “manganism,” which is similar to Parkinson’s disease. Fe is also involved in a variety of critical metabolic processes such as DNA synthesis, oxygen and electron transport, dopamine and serotonin synthesis, and myelin formation (9–11). Furthermore, it has been suggested that brain Fe content is critical for proper cognitive development and behavior (12,13). Increased total brain Fe content is associated with neurodegenerative disorders such as Alzheimer’s and Parkinson’s diseases (12), while Fe deficiency can also lead to developmental and intellectual retardation (12,14).

The precise mechanisms by which Mn and Fe are delivered into the brain, and how Mn and Fe affect each other’s disposition, are not clear. Mn and Fe share similar transporter systems that allow the metals to enter cells (e.g., transferrin, divalent metal transporter-1) (15). When the concentrations of the metals are high, there may be competition for the transporter or other targets between the ions so that changes in one metal may influence the distribution of the other. For example, Zheng *et al.* found that brain Fe metabolism was changed in rats exposed to high doses of Mn (16). Fe deficiency leads to increased Mn accumulation in the brain (17,18), while high Fe in the diet may decrease Mn absorption (19,20). There is also evidence that Mn and Fe may enter the brain through independent transport systems (21–26). It is well know that, in simple solutions, the water NMR relaxation rates (R_1 and R_2) are

directly proportional to the concentration of paramagnetic ion. This simple linear relationship has been widely used to estimate tissue levels of Mn or Fe alone using MRI (27–31). However, Mn and Fe are both paramagnetic, and they may compete or affect each other in biological systems. Thus the relationship between water relaxation rates and the concentrations of these paramagnetic ions together may not be as simple as assumed by the linear model. A more complex model may be needed to address the interaction between Mn and Fe binding and storage systems, and their combined effects on water relaxation times.

To address these questions, and to illustrate the need for more sophisticated analyses of imaging data, we studied the variations in MR relaxation rates as a function of metal content in groups of rats subjected to different combinations of dietary Fe and intravenous Mn. Our goal was to induce varying levels of both metals and to use quantitative MRI relaxometry to determine the Mn deposition pattern in different brain regions in rats exposed to this metal. In attempting to relate MR relaxation changes to tissue metal levels, we have developed a model that incorporates competitive mechanisms between the metal ions. Such a model is essential to explain our relaxation measurements.

MATERIALS AND METHODS

Animals

In order to achieve variable levels of Mn and Fe in tissues, adult male Sprague-Dawley rats were randomly separated into four groups; control (CN, n=5), Mn treated (MnT, n=6), Fe deficient and Mn treated (FeDMnT, n=6), Fe supplemented and Mn treated (FeSMnT, n=4) groups. MnT, FeDMnT, FeSMnT groups were given weekly intravenous (through tail vein) injections of a sterile isotonic Mn^{2+} solution ($MnCl_2$) equivalent to 3 mg Mn/kg body weight for a total of 14 weeks. This corresponds to doses of Mn comparable to those acquired by humans exhibiting symptoms of Mn intoxication (32). CN and MnT were maintained on a normal diet (30 mg Fe/kg chow, BioServe, Frenchtown, NJ, USA), while the FeDMnT and FeSMnT groups were given Fe deficient (3 mg Fe/kg feed; BioServe) or Fe supplemented (300 mg Fe/kg feed; BioServe) food, respectively. Food for all groups of rats has 12 mg Mn/kg chow. Fe in the Fe-supplemented diet (FeSMnT) was in the form of ferric citrate. Rats had free access to food and water throughout the study and were weighed weekly to monitor their general health. All procedures were in compliance with and approved by the Institutional Animal Care and Use Committee of Vanderbilt University.

MRI

Animals were scanned at the 14th week (24 h after the last Mn injection). All experiments were acquired using a 4.7T, 31-cm-horizontal-bore Varian INOVA magnet (Varian, Inc., Palo Alto, CA, USA) with actively shielded gradients (40 G/cm, rise times full amplitude of 130 μs) and a 63 mm transmit/receive quadrature imaging volume coil. Rat brains were scanned from both axial (FOV=40×40 mm, 30 slices) and coronal (FOV=40×50 mm, 20 slices) directions with 0.75 mm slice thickness.

Before the imaging procedure, animals were first anesthetized with isoflurane (2%) and placed in a stereotaxic support cradle with the head secured. The cradle was then put in the

volume coil to make sure the head of the animal was located at the center of the coil. Isoflurane was lowered to 1.5–1.75% and was maintained throughout the imaging experiment. Temperature (36.5–37.5°C) of the animal was monitored (SA Instruments, Stony Brook, NY, USA) and maintained via a flow of warm air which is controlled by a rectal temperature probe (SA Instruments). Respiration rates were externally monitored and maintained at 50–70 breaths per minute throughout the imaging session.

T_1 was measured using 2-D Fast Low Angle Shot sequences (FLASH) and different flip angles with parameters as follows: TR/TE=489/6.59 ms; flip angle=10, 30, 55, 70; 2 acquisitions. The image matrix was 256×256. T_2 was measured using a multislice fast spin echo (FSE) sequence: TR=5100 ms; Echo train length=8; k-space center=4; echo spacing=5, 6.7, 10, 13, 15 ms; 2 acquisitions; Image matrix=128×128.

T_1 and T_2 maps were calculated by fitting the series of T_1 and T_2 dependent images to the appropriate theoretical expressions using 2 parameter least squares fits. The parametric maps were then coregistered to a high resolution rat template and resliced using SPM (http://www.fil.ion.ucl.ac.uk/spm). Based on the rat brain template, multislice regions of interest (ROIs) were chosen for seven brain regions including cerebellum, brainstem, midbrain, striatum, hippocampus and cortex. Averaged T_1 and T_2 values within each of the ROIs were calculated for each rat and used in further analyses.

Multiple $MnCl_2$ phantoms with similar T_1 and T_2 values as the rat brain tissues were also made (pH 7). Their T_1 and T_2 values were measured at 37°C using an inversion recovery method and by changing TE in a spin echo sequence respectively.

Graphite furnace atomic absorption spectroscopy (GFAAS)

At the conclusion of the study, the animals were euthanized and their brains were removed, dissected (into cerebellum, brainstem, midbrain, striatum, hippocampus, and cortex), weighed and quick frozen. Tissue Mn and Fe were measured in these regions with GFAAS (Varian AA240, Varian, Inc.). Brain regions were digested in ultrapure nitric acid (1:10 w/v dilution) for 48–72 h in a sandbath (60°C). An aliquot of 100 μl of digested tissue was brought to 1 ml total volume with 2% nitric acid and analyzed for Mn and Fe. Both Mn and Fe GFAAS analyses were performed at the same time in the same sample. The standards used to standardize the GFAAS were purchased from Acros Organics, Morris Plains, NJ, USA: Mn (#19611–1000) and Fe (#19605–1000). Bovine Liver Standard (National Bureau of Standards, Washington, DC) was used as external standard in every analysis.

Statistical analysis

Levene's homogeneity-of variance test was first applied to test if the variances are equal across groups ($p<0.05$). One-way ANOVA was used to determine if differences exist among the group means at an alpha level of 0.05. If significant difference was detected among the means, post-hoc range tests (Tukey HSD if variances are equal across groups, Dunnett T3 if variances are unequal across groups) were then applied to test the difference between each pair of means at an alpha level of 0.05. All statistical analyses were performed with SPSS software (SPSS, Inc., Chicago, IL, USA).

RESULTS

Experiment results

Ion concentrations measured by GFAAS—Averaged metal concentrations at six brain regions which were measured by GFAAS at the 14th week for the four groups of rats are summarized in Table 1a (Mn concentration) and Table 1b (Fe concentration). One-way ANOVA and post-hoc range tests were used to compare Mn and Fe levels in each brain region across groups (see details in Materials and Methods Section).

Brain Mn levels were statistically significantly higher in the cerebellum and brainstem for all treated animals (MnT, FeDMnT, and FeSMnT) compared to CN ($p<0.05$). Other brain regions showed differential metal dysregulation compared to CN animals. For example, Mn content was increased in the hippocampus of MnT animals ($p<0.01$), but decreased in animals receiving FeDMnT chow ($p<0.05$). Additionally, cortical Mn concentrations were greater in FeDMnT and FeSMnT ($p<0.05$) compared to control animals, while MnT animals had cortical Mn concentrations similar to CN.

Brain Fe content was also determined at the conclusion of the study. No significant change in Fe concentration was observed between the CN and MnT groups in any of the examined brain regions (Table 1b). Brain Fe levels were also indistinguishable in animals receiving Fe-modified diets regardless of whether animals were FeD or FeS chow. Additionally, cerebellar Fe was statistically significantly lower in FeSMnT and FeDMnT animals compared to either CN or MnT ($p<0.05$). No differences in Fe concentrations were observed in the hippocampus, midbrain or striatum among the four groups. Finally, the FeDMnT group demonstrated a statistically significant decrease in Fe deposition in the cortex relative to MnT ($p<0.05$), and in the cerebellum and brainstem compared to both the MnT and CN ($p<0.05$ for both groups).

Relaxation rates measured by MRI—Typical axial and coronal T_1 weighted images of control and Mn-treated rats at week 14 are presented in Fig. 1 (1st and 2nd columns of Fig. 1a and b). Pronounced signal increases are apparent in specific brain regions, such as the pontine nuclei (pons) (Fig. 1a, first and second rows, white arrow), dentate gyrus (Fig. 1b, black arrow and circle) and habenula (Fig. 1a, forth row, white arrow). The contrast of T_1-weighted images was increased in brain regions, such as hippocampus (Fig. 1a, balck arrow), pontine nuclei (Fig. 1a, first and second rows, white arrow), cerebellum (CB) (Fig. 1b, 3rd row) and olfactory bulb (OB) (Fig. 1b, 4th row), allowing clear visualization of anatomic details of the brain neuroarchitecture. The CA3 layer of hippocampus, as well as layers of olfactory bulb was also clearly distinguishable in Mn treated rats due to the signal and contrast enhancement. Improved gray-white matter contrast was also apparent in the cerebellum. These increases in T_1 weighted signal and contrast were similar to those previously reported (4,33,34).

As seen in the T_1-weighted images (3rd and 4th columns of Fig. 1a,b), the signal and contrast enhancement effects in the FeDMnT and FeSMnT groups were similar to those shown in the MnT group. The FeDMnT and FeSMnT groups had higher Mn deposition in

most brain regions so the MRI signal enhancement was likely due to Mn accumulation in the brain.

One-way ANOVA and post-hoc range tests (see details above) were used to compare the difference of R_1 and R_2 values among the four groups in different brain regions. Average R_1 and R_2 values for the four groups and the results of the statistical tests are summarized in Table 2.

Compared to the CN group, significant increases in R_1 were observed in the MnT group in all brain regions ($p<0.001$) except the brainstem and cortex. No significant differences of R_1 values were observed between the FeDMnT and FeSMnT groups in any of the examined brain regions. However, R_1 values of the FeDMnT and FeSMnT groups were significantly larger than the values of CN and MnT groups (Table 2a,b).

Significant differences in R_2 between the CN and MnT groups were observed only in the striatum ($p=0.01$). No significant differences in R_2 values were observed between the FeDMnT and FeSMnT groups in any of the brain regions except hippocampus ($p=0.03$), while it approached significance in cerebellum ($p=0.07$). The FeSMnT group showed increased R_2 values in these regions compared to the FeDMnT group. Compared with the CN group, the FeDMnT and FeSMnT groups showed significant increases in R_2 in the brainstem and striatum ($p<0.01$). While no significant differences of R_2 values were observed between the FeDMnT group and the MnT group in any of the brain regions except for the brainstem ($p=0.037$), the FeSMnT group showed significant increase in multiple brain regions including the cortex, striatum and cerebellum ($p<0.01$) compared to the MnT group. Detailed experimental results have been previously reported by Fitsanakis *et al.* (35).

Model construction

The experimental results revealed that both Mn and Fe concentrations measured by GFAAS, as well as the R_1 and R_2 values, measured by MRI, varied across groups and across regions in a complicated way. Such effects imply that the relationship between relaxation rate and concentration may vary among tissues and complicate the use of relaxometry for estimating metal levels. We therefore evaluated two questions: (a) What is the relationship between the Mn (and/or Fe) concentration and R_1 (and/or) R_2? (b) Is MRI a reliable methodology to predict the metal concentrations in the brain? We used two different models to answer these questions.

Linear model—In simple aqueous solutions a linear relationship exists between the concentration of a paramagnetic species and the relaxation rate R_1 ($1/T_1$) and R_2 ($1/T_2$):

$$R_{1,2}([\text{ lon }]) = R_{1,2}(0) + r_{1,2}[\text{ lon }] \quad (1)$$

where $R_{1,2}$([Ion]) is the MRI measured relaxation rate at a given concentration of paramagnetic ion and $r_{1,2}$ is the so-called relaxivity. Taking Mn^{2+} as an example, $R_{1,2}(0)$ is the water proton relaxation rates without Mn^{2+}, and the constant $r_{1,2}$ can be determined by fitting experimental data to eqn (1) (4,5,36). Thus, tissues with higher concentrations of Mn should have shorter relaxation times and show higher signal intensity in T_1-weighted

images, and lower signal intensity in T_2-weighted images. Note that the absolute quantification of Mn levels is not straightforward because the relaxivity r is not an intrinsic property of the metal ion alone. The relaxivity may change with the specific molecular form and environment in which the metal resides. For example, it may increase as a result of binding to intracellular ligands (5,37), or it may decrease if the metal's electron structure is altered or water access to the metal is restricted, as occurs in many molecular configurations. Quantification of the ratio r_2/r_1 may also provide insights into the chemical form of the metal (5).

Control (CN) and Mn-treated with normal diet (MnT) groups.: As shown in the experimental results, no difference in Fe concentrations existed between the control and the Mn-treated with normal diet (MnT) groups in any of the brain regions (Table 1b). For these two groups, we assumed that changes in Mn concentrations were the main contribution to the changes in the MR relaxation rates. Thus, the above linear model (eqn 1) was first applied only to these two groups.

As illustrated in Fig. 2a,b the relaxation rates in most tissues in the CN and MnT groups increased linearly with increased Mn levels. The slopes (the effective relaxivities), however, varied in different regions and were all much smaller than the relaxivities of simple aqueous solutions. Midbrain and cortex showed negative r_1 and r_2 values respectively, which has no physical meaning, though the correlations between relaxation rate and concentration were not significant (Table 3a,b). In addition, the ratio of R_2 relaxivity (r_2) to R_1 relaxivity (r_1) also varied among tissues and it was less than the ratio of the aqueous solution in all brain regions (Table 3c).

The increases in relaxation rates were likely due to the deposition of Mn in the brain, though other contributions might be present, for example, from associated changes in Fe. The observation that Mn relaxivity varied among regions suggests the metal exists in different forms, or is physically confined to different degrees in different areas. Conversion of Mn^{2+} to another oxidation state of the metal, the presence of different substrates for binding, the effects of competition from other metals, as well as the variation in micro-viscosity, may all influence the relaxivity (5,37). Similarly, the r_2/r_1 ratio suggests there are differences in chemical form and binding effects. In the hippocampus, the R_1 and R_2 relaxivity were both small, although the metal levels there were relatively high. This implies that the relaxation effect of the Mn as a paramagnetic ion is largely decreased, as would be expected if Mn^{2+} is converted to a less paramagnetic state or if water access to the ion is restricted. These regional variations may be important for the interpretation of MR methods in use for tracking neural connectivity and for the use of MRI for monitoring metal deposition in tissues.

All four groups.: When the dietary Fe levels were varied, the amount of both Mn and Fe in the brain changed, as shown in Table 1. The absolute levels of Fe did not necessarily agree with the expected amounts from dietary intake, but for the purposes of determining how the levels of the two metals varied compared to each other, we needed only to achieve differing levels of the respective metals. We tried to test the utility of the linear model in two ways. First, relaxation rates were plotted against Mn and Fe concentrations separately using eqn

(1). The fitting results are shown in Figure 2c–f and summarized in Table 4. Second, we assumed that both Mn and Fe independently exist in the brain, so that the relaxation rates measured by MRI are just a linear combination of their contributions, as shown in eqns (2) and (3). The least squares fitting method was applied to find the coefficients with the minimum residual. The results are summarized in Table 5.

$$R_1([\mathrm{Mn}],[\mathrm{Fe}]) = R_1(0) + r_{1,\mathrm{Mn}}[\mathrm{Mn}] + r_{1,\mathrm{Fe}}[\mathrm{Fe}] \quad (2)$$

$$R_2([\mathrm{Mn}],[\mathrm{Fe}]) = R_2(0) + r_{2,\mathrm{Mn}}[\mathrm{Mn}] + r_{2,\mathrm{Fe}}[\mathrm{Fe}] \quad (3)$$

As shown in Fig. 2c–f and Tables 4 and 5, the estimated apparent longitudinal relaxivities of Fe were negative for most of the brain regions, which has no clear physical interpretation. Most of these negative values are highly significant as the corresponding p (significance) values are much smaller than 0.05 (Tables 4 and 5). These data indicate these negative values were mainly due to inappropriate application of the linear model and its incapacity to deal with simultaneous variations in two paramagnetic ions at the same time. The failure of the linear model and the results of GFAAS both suggested that Mn and Fe interact competitively and their combined influence on relaxation rates are more complicated than can be predicted with such a simple model.

Competition model

We propose a new model (Fig. 3 and eqns 4–12) to explain and interpret the combined influence of Mn and Fe on tissue relaxation rates. As illustrated in Fig. 3, we assume Mn and Fe compete for a common specific binding site or a set of sites. We also assume that in a given brain region, Mn or Fe can either be bound to this common binding site (MnB or FeB) or be “else” (called MnE or FeE), as shown in eqns (6) and (7). Here, the “else” ions include free ions and ions that bind to other substrates without competition. When either MnE or FeE successfully binds to a free common binding site (BS_{free}), they become MnB (1 Mn ion plus 1 common binding site) or FeB (1 Fe ion plus 1 common binding site), as shown in eqns (4) and (5). In a steady state, chemical equilibrium will be achieved between free ions, bound ions and common binding sites (eqns 4 and 5). The two equilibrium constants $K_{eq,Mn}$ and $K_{eq,Fe}$ are used to describe the chemical equilibrium for Mn and Fe respectively (eqns 9 and 10). The total number of common binding sites (BS_{total}) is the summation of three parts: free binding sites (BS_{free}), sites that bind to Mn (as in MnB) and sites that bind to Fe (as in FeB), as shown in eqn (8). Mn_{total} and Fe_{total} are the total Mn and Fe metals contents measured by GFAAS. The longitudinal and transverse relaxation rates R_1 and R_2 are a linear combination of the effects of MnB, FeB, MnE, and FeE as described by eqns (11) and (12). The parameters in eqns (6)–(12) can be estimated by a least-squares method. First, a set of initial values are given, then the nonlinear equations are solved by the Levenberg–Marquardt method (38) using the initial values of parameters and the values of measured Mn and Fe concentrations for each individual rat. Next, $R_1(0)$ and relaxivities are fitted using the measured R_1 data according to eqn (11). The algorithm is a subspace trust region method and is based on the interior-reflective Newton method described in Ref. (39). Once the convergence criteria are met and the eight parameters ($K_{eq,Mn}$, $K_{eq,Fe}$, [BS_{total}], $R_1(0)$,

$r_{1,MnB}$, $r_{1,MnE}$, $r_{1,FeB}$, $r_{1,FeE}$) are updated, the above procedure is repeated until a local minimum of residual error is found. Boundaries were set for the relaxivities during the fitting procedure to assure that their values are positive. The nonlinear fitting procedure in the proposed method requires careful consideration of initial parameter values and boundaries, which are common requirements for nonlinear optimization problems in mathematics. Additionally, as stated previously, the negative relaxivity has no physical meaning and accordingly must be properly handled to ensure computational validity. No convergence problems were encountered during the fitting procedures or the calculations. The stability/reproducibility depends on the initial values of the fitting parameters, which is a common problem for most of the nonlinear fitting models. The existence of local minima affects the reproducibility of fitting with different initial values. The Monte Carlo simulation scheme is used to randomly set initial values and to search for the global minimum. Best simulation results are chosen based on statistical parameters, that is, R^2 of the fitting procedure. This makes the proposed methodology more robust and objective.

After the R_1 fitting procedure is accomplished and eqns (6)–(11) are solved, MnB, MnE, FeB, and FeE concentrations are derived for each rat. Transverse relaxivities are then calculated using eqn (12). We chose to fit eqn (11) first rather than 12 based on the following rationale: First, the longitudinal relaxation rate correlates with Mn and Fe concentrations better than the transverse relaxation rate (Fig. 2 and Tables 3–5). This effect is consistent with what has been reported in the literature. For example, Southon *et al.* (40) reported that, in rat liver and pig organs, both MnDPDP and $MnCl_2$ produced a positive dose-response in R_1 and tissue Mn concentration, and only small or no response in R_2. The effect of Fe on the transverse and longitudinal relaxation rates is complicated and has been reported in the literature in different ways. Although Fe is believed to be an effective T_2 weighted contrast agent, it has been reported that Fe (III) changes $T_2 < T_1$ (41). Multiple factors like the pH, ion-binding capacity and the chemical form of the ion can influence effect of metal ions on proton relaxation in a complicated fashion. The fact that T_1 maps (256×256) have higher resolution than T_2 maps (128×128) is another reason for us to select R_1 instead of R_2. The fitting results are summarized in Tables 6 and 7.

$$\mathrm{MnE} + \mathrm{BS}_{\mathrm{free}} \xrightarrow{K_{\mathrm{eq,Mn}}} \mathrm{MnB} \tag{4}$$

$$\mathrm{FeE} + \mathrm{BS}_{\mathrm{free}} \xrightarrow{K_{\mathrm{eq,fe}}} \mathrm{FeB} \tag{5}$$

$$[\mathrm{Mn}_{\mathrm{total}}] = [\mathrm{MnB}] + [\mathrm{MnE}] \tag{6}$$

$$[\mathrm{Fe}_{\mathrm{total}}] = [\mathrm{FeB}] + [\mathrm{FeE}] \tag{7}$$

$$[\mathrm{BS}_{\mathrm{total}}] = [\mathrm{MnB}] + [\mathrm{FeB}] + [\mathrm{BS}_{\mathrm{free}}] \tag{8}$$

$$K_{\mathrm{eq,Mn}} = \frac{[\mathrm{MnB}]}{[\mathrm{MnE}][\mathrm{BS_{free}}]} \tag{9}$$

$$K_{\mathrm{eq,Fe}} = \frac{[\mathrm{FeB}]}{[\mathrm{FeE}][\mathrm{BS_{free}}]} \tag{10}$$

$$R_1 = R_1(0) + r_{1,\mathrm{MnB}}[\mathrm{MnB}] + r_{1,\mathrm{MnE}}[\mathrm{MnE}] + r_{1,\mathrm{FeB}}[\mathrm{FeB}] + r_{1,\mathrm{FeE}}[\mathrm{FeE}] \tag{11}$$

$$R_2 = R_2(0) + r_{2,\mathrm{MnB}}[\mathrm{MnB}] + r_{2,\mathrm{MnE}}[\mathrm{MnE}] + r_{2,\mathrm{FeB}}[\mathrm{FeB}] + r_{2,\mathrm{FeE}}[\mathrm{FeE}] \tag{12}$$

As shown in Table 6, the increase in relaxation rates was most likely due to the bound Mn and bound Fe since the relaxivities of FeE and MnE were very small, suggesting chemical modification and/or compartmentation. In Table 6, the symbol “Null” indicates the fitting parameter value is zero. It appears that the effect of MnB is significant for both r_1 and r_2 in all brain regions. In most of the brain regions, Mn that was bound to the common binding site showed a larger relaxation effect than the bound Fe, as r_1 and r_2 of MnB were much larger than the ones for FeB. The effect of FeE is not significant in most of the brain regions, except in the cortex. In the striatum and brainstem, the longitudinal and transverse relaxivites of Fe (both FeB and FeE) were zero, suggesting that Fe may have existed in a nonparamagnetic state or its paramagnetic character was largely diminished in these brain regions. The r_1 relaxivities of bound Fe in the hippocampus were much larger than in the other brain regions. Due to limited data, a more rigorous statistical analysis requires future theoretical and experimental work.

The predicted regional tissue concentrations of MnB, MnE, FeB, and FeE were also derived for each rat. The averaged values for CN, MnT, FeSMnT and FeDMnT groups are summarized in Table 7. Regional variations were also observed. For example, in the midbrain, most of the common binding sites were occupied by both Mn and Fe. In cerebellum, most of the common binding sites were occupied by Fe in all four groups (CN, MnT, FeSMnT, FeDMnT). The amount of FeB and MnB was consistent among the four groups while the FeE concentration decreased more than 85% in FeSMnT and FeDMnT groups compared to CN and MnT groups. The hippocampus was different from other regions as the ratio of [MnB]/[FeB] approximated 1:1, and it was consistent for all four groups. In addition, most of the Fe in the hippocampus was not bound to the common binding sites.

Figure 4 shows the fitting results of the interacting model. The measured and predicted relaxation rates in all brain regions were plotted against ion concentrations (Fig. 4a–d). In addition, predicted relaxation rates in all brain regions were plotted against measured values (Fig. 4e and f). The nonlinear relationships between relaxation rates and [Mn] as well as relaxation rates with [Fe] appear to be well explained by this model. Note that the transverse relaxation rate is less well fitted than the longitudinal relaxation rate (Fig. 4e and f).

DISCUSSION

Comparison of the competition model with the linear models

The fits to the data for the linear and competition models have been compared. The corresponding correlation coefficient, 95% confidence interval of the correlation coefficient as well as the *p* values are summarized in Table 8. Also, the regressions for all brain regions for all four models (competition model, linear model with both Mn and Fe considered, linear model with only Mn considered, linear model with only Fe considered) are plotted in Fig. 5. As illustrated in Fig. 5a, the competition model and the linear model with Mn and Fe fitted together using eqn (2) provided the best r^2 in all of the brain regions. In some brain regions the fits derived by these two models are significantly improved over the other two linear models in which only one ion is considered (eqn 1). For example, for striatum the correlation coefficients derived by the competition and the linear models with both Mn and Fe considered are 0.87 and 0.85 respectively, while the values for the other two linear models with either Mn or Fe considered are 0.69 and 0.02 with 95% confidence interval of [0.36, 0.86] and [−0.42, 0.45] respectively. Other brain regions, like brainstem and midbrain, also provide evidence that the competition and the linear models, taking into account both Mn and Fe, provide better fitting results than one or both of the other two linear models. There is no significant difference between the correlation coefficients of the competition model and the linear model with both Mn and Fe counted. However, as shown above, the relaxivities of Fe fitted with the linear model are significantly negative in almost all of the brain regions (Table 5) which does not have any physical meaning. Thus, considering one metal alone at a time or both metals acting independently fails either to provide physically interpretable fits or to fit the data very successfully. Only by considering the competitive model are reasonable fits that have physical meanings obtained.

The supplied chow for the different groups of rats all came from the same source (BioServe) and is formulated according to the AIN-93 guidelines for rodent chow to ensure proper health. The metal/mineral content was analyzed prior to shipment. Accordingly, the reported values are deemed reliable. A diet with Fe overload is known to increase Fe accumulation in the plasma (42). The increased brain Mn concentration accompanied by decreased brain Fe concentration with Fe supplemented in diet is surprising. This may be due to the fact that the added Mn that is on board in the FeSMnT group is more readily taken into the brain, offsetting the Fe overload in the diet. Alternatively, it is possible that Fe overload in the cells prevents the extracellular extrusion of Mn. Fe is transported extracellularly by ferroportin, and it has yet to be determined whether Mn shares the same transporter. If so, the Mn that is in the cells may be trapped due to the abundant Fe concentration in animals treated with fortified Fe diet, accounting for increased brain Mn levels in conditions of Fe repletion. This is well beyond the scope of this manuscript, but studies to assess the possibility are currently under way.

Similar studies where rats were overloaded with dietary Fe for extended periods of time have been associated with approximately 10-fold increases in plasma Fe levels (43,44). This is likely due to the inability of the regulatory mechanisms to accurately adapt to the brain's Fe requirements, due to transport and storage of Fe in ferritin. Normally, in the presence of

exceedingly high levels of Fe, the regulatory pathway perceives the central nervous system as Fe deficient, despite excessive Fe accumulation, and Fe uptake into the brain continues. When Fe regulatory protein-1 (IRP1) and IRP2 bind to the Fe regulatory element (IRE) in the 3′-untranslated region of transferrin receptor (TfR) or DMT1 mRNA, the transcript is stabilized, translation proceeds, and the proteins are synthesized. Thus, a high IRP binding activity reflects low body Fe stores and results in up-regulation of DMT1 and TfR. Vice versa, high intracellular Fe concentrations are predicted to have an opposite effect. Nonetheless, it is possible that down-regulation of DMT1 and TfR is associated with up-regulation of transporters that are Mn-specific. Thus even in the presence of high Fe, the uptake of Mn may continue unabated. It has also been reported by Chua and Morgan that iron overload and deficiency led to increased brain Mn (17).

Regional variation of the relaxivities and combined influence of Mn and Fe on MRI signal

One of our observations is that Mn and Fe relaxivities varied among various brain regions, suggesting that these metals exist in different forms or bind to different substrates. For example, the relaxivity of Mn can be decreased when Mn^{2+} is converted to a less paramagnetic state or if water access to the ion is restricted. The relaxation properties of iron can also be varied as its putative storage protein, ferritin, has different clustering stages and the concentration of ferritin varies in different brain regions (45,46). The effects of competition from other metals, as well as the variation in micro-viscosity may all influence the metal relaxivity (5,37).

The effects of Mn and Fe on MR relaxation rates have been studied before in isolation and without consideration of the potential interaction between the two (27–29,31). Thus, when studies are designed to examine the effect of Mn on relaxivities, no other metal ions are usually considered. Conversely, other studies that focus solely on Fe have failed to take into account the interrelationship of this metal with Mn. As a result, most researchers have used a linear model to explain the influence of paramagnetic ions on the MRI signal. Our results show that when only one paramagnetic ion concentration change occurs, the simple linear model may appear to explain the relationship between ion concentration and relaxation rates. Thus the relaxation rate measured by MRI can be used as an indicator of ion concentration for this case. However, even with this simple linear model, the relaxivities vary among regions, implying that different brain regions should be treated separately rather than taking the whole brain as a single homogeneous region. To our knowledge, our study is the first one to examine the regional variation of the relaxivities.

Although Mn and Fe are commonly studied together in the toxicology field, no MRI study was found in the literature to report on the combined influence of Mn and Fe on MRI signals. Our study is the first one to investigate this effect. Our results reveal that when more than one paramagnetic ion concentration is changing, the linear model does not describe the effects properly. As a result, a more complicated model must be applied. We propose an interacting model based on the fact that Mn and Fe may compete *in vivo* and both of them will affect MRI signals (5,21,37). These important regional variation effects are still very apparent in the interacting model.

CONCLUSION

It has been shown above, when Mn and Fe concentrations are both altered in a biological system, that their combined influence on MRI signals is complicated. In such a case, the simple linear model for explaining the relationship between MRI signal and a single changed paramagnetic ion will not be suitable to explain the change in MRI relaxation rates. Regional variations are apparent in both the experimental data and the model. Although the proposed competition model, like most nonlinear optimization problem, has its limitations and uncertainty, such as careful selection of initial parameter values and boundaries, proper convergence criteria for the balance of computational cost and accuracy, global and local minimum, this represents a first attempt to explain the interacting relationship of two paramagnetic ions and their influence on the MRI signals. Our model correctly predicts the nonlinear relationship between relaxation rates and ion contents. This model may be useful for interpreting MR results when more than one paramagnetic species is involved.

Acknowledgements

We would like to thank Richard Baheza for his assistance with MRI data acquisition, Jarrod True and Jennifer Begtrup for animal care assistance and Joel G. Anderson for GFAAS data acquisition and analysis. This work was supported by DoD Manganese Health Research Project 04149002 and NIEHS ES 007331 (M.A.).

Abbreviations used:

95% CI	95% confidence interval
BS	brainstem
BS_{total}	total number of common binding sites
BS_{free}	free binding sites
CB	cerebellum
CC	correlation coefficient
CX	cortex
CN	control group
DG	dentate gyrus
FeB	bound iron (binds to a common binding site)
FeDMnT	manganese treated group fed with iron deficient food
FeE	iron exists in other format (either free or binds to uncommon binding site)
FeSMnT	manganese treated group fed with iron supplemented food
FOV	field of view
Hb	habenula

HDL	high density lipoprotein
HP	hippocampus
K_{eq}	equilibrium constant
MB	midbrain
MnB	bound manganese (binds to a common binding site)
MnE	manganese exists in other format (either free or binds to uncommon binding site)
MnT	manganese treated group with normal diet
MRI	magnetic resonance imaging
pons	pontine nuclei
ST	striatum

REFERENCES

1. Fitsanakis VA, Zhang N, Avison MJ, Gore JC, Aschner JL, Aschner M. The use of magnetic resonance imaging (MRI) in the study of manganese neurotoxicity. Neurotoxicology 2006; 27(5): 798–806. [PubMed: 16620989]
2. Bloembergen N, Purcell EM, Pound RV. Relaxation effects in nuclear magnetic resonance absorption. Phys. Rev 1948; 73(7): 679–712.
3. Gore JC, Kennan RP. Contrast agents and relaxation effects. In Magnetic resonance imaging of the brain and spine, 2nd ed. Atlas SW (ed). Lippincott-Raven Press: Philadelphia, 1996; 89–107.
4. Silva AC, Lee JH, Aoki I, Koretsky AP. Manganese-enhanced magnetic resonance imaging (MEMRI): methodological and practical considerations. NMR Biomed. 2004; 17(8): 532–543. [PubMed: 15617052]
5. Kang YS, Gore JC, Armitage IM. Studies of factors affecting the design of NMR contrast agents: manganese in blood as a model system. Magn. Reson. Med 1984; 1(3): 396–409. [PubMed: 6443783]
6. Erikson KM, Aschner M. Manganese neurotoxicity and glutamate-GABA interaction. Neurochem. Int 2003; 43(4–5): 475–480. [PubMed: 12742094]
7. Fitsanakis VA, Aschner M. The importance of glutamate, glycine, and gamma-aminobutyric acid transport and regulation in manganese, mercury and lead neurotoxicity. Toxicol. Appl. Pharmacol 2005; 204(3): 343–354. [PubMed: 15845423]
8. Greger JL. Nutrition versus toxicology of manganese in humans: evaluation of potential biomarkers. Neurotoxicology 1999; 20(2–3): 205–212. [PubMed: 10385884]
9. Rouault TA. Systemic iron metabolism: a review and implications for brain iron metabolism. Pediatr. Neurol 2001; 25(2): 130–137. [PubMed: 11551743]
10. Lieu PT, Heiskala M, Peterson PA, Yang Y. The roles of iron in health and disease. Mol. Aspects Med 2001; 22(1–2): 1–87. [PubMed: 11207374]
11. Connor JR, Menzies SL. Relationship of iron to oligodendrocytes and myelination. GLIA 1996; 17(2): 83–93. [PubMed: 8776576]
12. Sipe JC, Lee P, Beutler E. Brain iron metabolism and neurodegenerative disorders. Dev. Neurosci 2002; 24(2–3): 188–196. [PubMed: 12401958]
13. Felt BT, Lozoff B. Brain iron and behavior of rats are not normalized by treatment of iron deficiency anemia during early development. J. Nutr 1996; 126(3): 693–701. [PubMed: 8598555]

14. Pollitt E, Leibel RL. Iron deficiency and behavior. J. Pediatr 1976; 88(3): 372–381. [PubMed: 1107503]
15. Erikson KM, Shihabi ZK, Aschner JL, Aschner M. Manganese accumulates in iron-deficient rat brain regions in a heterogeneous fashion and is associated with neurochemical alterations. Biol. Trace Elem. Res 2002; 87(1–3): 143–156. [PubMed: 12117224]
16. Zheng W, Zhao Q, Slavkovich V, Aschner M, Graziano JH. Alteration of iron homeostasis following chronic exposure to manganese in rats. Brain Res. 1999; 833(1): 125–132. [PubMed: 10375687]
17. Chua AC, Morgan EH. Effects of iron deficiency and iron overload on manganese uptake and deposition in the brain and other organs of the rat. Biol. Trace Elem. Res 1996; 55(1–2): 39–54. [PubMed: 8971353]
18. Kwik-Uribe CL, Gietzen D, German JB, Golub MS, Keen CL. Chronic marginal iron intakes during early development in mice result in persistent changes in dopamine metabolism and myelin composition. J. Nutr 2000; 130(11): 2821–2830. [PubMed: 11053527]
19. Davis CD, Wolf TL, Greger JL. Varying levels of manganese and iron affect absorption and gut endogenous losses of manganese by rats. J. Nutr 1992; 122(6): 1300–1308. [PubMed: 1588448]
20. Finley JW. Manganese absorption and retention by young women is associated with serum ferritin concentration. Am. J. Clin. Nutr 1999; 70(1): 37–43. [PubMed: 10393136]
21. Malecki EA, Devenyi AG, Beard JL, Connor JR. Existing and emerging mechanisms for transport of iron and manganese to the brain. J. Neurosci. Res 1999; 56(2): 113–122. [PubMed: 10777372]
22. Banks WA, Kastin AJ, Fasold MB, Barrera CM, Augereau G. Studies of the slow bidirectional transport of iron and transferrin across the blood-brain barrier. Brain Res. Bull 1988; 21(6): 881–885. [PubMed: 3224280]
23. Crowe A, Morgan EH. Iron and transferrin uptake by brain and cerebrospinal fluid in the rat. Brain Res 1992; 592(1–2): 8–16. [PubMed: 1450923]
24. Morris CM, Keith AB, Edwardson JA, Pullen RG. Uptake and distribution of iron and transferrin in the adult rat brain. J. Neurochem 1992; 59(1): 300–306. [PubMed: 1613505]
25. Dickinson TK, Devenyi AG, Connor JR. Distribution of injected iron 59 and manganese 54 in hypotransferrinemic mice. J. Lab. Clin. Med 1996; 128(3): 270–278. [PubMed: 8783634]
26. Malecki EA, Devenyi AG, Beard JL, Connor JR. Transferrin response in normal and iron-deficient mice heterozygotic for hypotransferrinemia; effects on iron and manganese accumulation. Biometals 1998; 11(3): 265–276. [PubMed: 9850571]
27. Kim SH, Chang KH, Chi JG, Cheong HK, Kim JY, Kim YM, Han MH. Sequential change of MR signal intensity of the brain after manganese administration in rabbits. Correlation with manganese concentration and histopathologic findings. Invest. Radiol 1999; 34(6): 383–393. [PubMed: 10353030]
28. Gallez B, Demeure R, Baudelet C, Abdelouahab N, Beghein N, Jordan B, Geurts M, Roels HA. Non invasive quantification of manganese deposits in the rat brain by local measurement of NMR proton T_1 relaxation times. Neurotoxicology 2001; 22(3): 387–392. [PubMed: 11456339]
29. Dorman DC, Struve MF, Wong BA, Dye JA, Robertson ID. Correlation of brain magnetic resonance imaging changes with pallidal manganese concentrations in rhesus monkeys following subchronic manganese inhalation. Toxicol. Sci 2006; 92(1): 219–227. [PubMed: 16638924]
30. Chaki H, Furuta S, Matsuda A, Yamauchi K, Yamamoto K, Kokuba Y, Fujibayashi Y. Magnetic resonance image and blood manganese concentration as indices for manganese content in the brain of rats. Biol. Trace Elem. Res 2000; 74(3): 245–257. [PubMed: 11055811]
31. House MJ, St Pierre TG, Kowdley KV, Montine T, Connor J, Beard J, Berger J, Siddaiah N, Shankland E, Jin LW. Correlation of proton transverse relaxation rates (R_2) with iron concentrations in postmortem brain tissue from alzheimer's disease patients. Magn. Reson. Med 2007; 57(1): 172–180. [PubMed: 17191232]
32. Mergler D, Baldwin M, Belanger S, Larribe F, Beuter A, Bowler R, Panisset M, Edwards R, de Geoffroy A, Sassine MP, Hudnell K. Manganese neurotoxicity, a continuum of dysfunction: results from a community based study. Neurotoxicology 1999; 20(2–3): 327–342. [PubMed: 10385894]

33. Lee JH, Silva AC, Merkle H, Koretsky AP. Manganese-enhanced magnetic resonance imaging of mouse brain after systemic administration of $MnCl_2$: dose-dependent and temporal evolution of T_1 contrast. Magn. Reson. Med 2005; 53(3): 640–648. [PubMed: 15723400]
34. Watanabe T, Frahm J, Michaelis T. Functional mapping of neural pathways in rodent brain in vivo using manganese-enhanced three-dimensional magnetic resonance imaging. NMR Biomed. 2004; 17(8): 554–568. [PubMed: 15617054]
35. Fitsanakis VA, Zhang N, Anderson JG, Erikson KM, Avison MJ, Gore JC, Aschner M. Measuring brain manganese and iron accumulation in rats following 14 weeks of low-dose manganese treatment using atomic absorption spectroscopy and magnetic resonance imaging. Toxicol. Sci 2008; 103(1): 116–124. [PubMed: 18234737]
36. Nordhoy W, Anthonsen HW, Bruvold M, Brurok H, Skarra S, Krane J, Jynge P. Intracellular manganese ions provide strong T_1 relaxation in rat myocardium. Magn. Reson. Med 2004; 52(3): 506–514. [PubMed: 15334568]
37. Gore JC. Physical factors in the design of contrast agents for MRI. IEEE Eng. Med. Biol 1985; 4(3): 39–42.
38. Marquardt D An algorithm for least-squares estimation of nonlinear parameters. SIAM J. Appl. Math 1963; 11: 431–441.
39. Coleman TF, Li Y. On the convergence of reflective newton methods for large-scale nonlinear minimization subject to bounds. Math. Progr 1994; 67(2): 189–224.
40. Southon TE, Grant D, Bjornerud A, Moen OM, Spilling B, Martinsen I, Refsum H. NMR relaxation studies with MnDPDP. Acta Radiol 1997; 38(4 Pt 2): 708–716. [PubMed: 9245966]
41. Barnhart JL, Berk RN. Influence of paramagnetic ions and pH on proton NMR relaxation of biologic fluids. Invest. Radiol. 1986; 21(2): 132–136.
42. Klevay LM. Iron overload can induce mild copper deficiency. J. Trace Elem. Med. Biol 2001; 14(4): 237–240. [PubMed: 11396784]
43. Dabbagh AJ, Mannion T, Lynch SM, Frei B. The effect of iron overload on rat plasma and liver oxidant status in vivo. Biochem. J 1994; 300(Pt 3): 799–803. [PubMed: 8010963]
44. Bacon BR, Tavill AS, Brittenham GM, Park CH, Recknagel RO. Hepatic lipid peroxidation in vivo in rats with chronic iron overload. J. Clin. Invest 1983; 71(3): 429–439. [PubMed: 6826715]
45. Gossuin Y, Gillis P, Muller RN, Hocq A. Relaxation by clustered ferritin: a model for ferritin-induced relaxation in vivo. NMR Biomed 2007; 20(8): 749–756. [PubMed: 17330925]
46. Vymazal J, Brooks RA, Bulte JWM, Gordon D, Aisen P. Iron uptake by ferritin: NMR relaxometry studies at low iron loads. J. Inorg. Biochem 1998; 71(3–4): 153–157. [PubMed: 9833320]

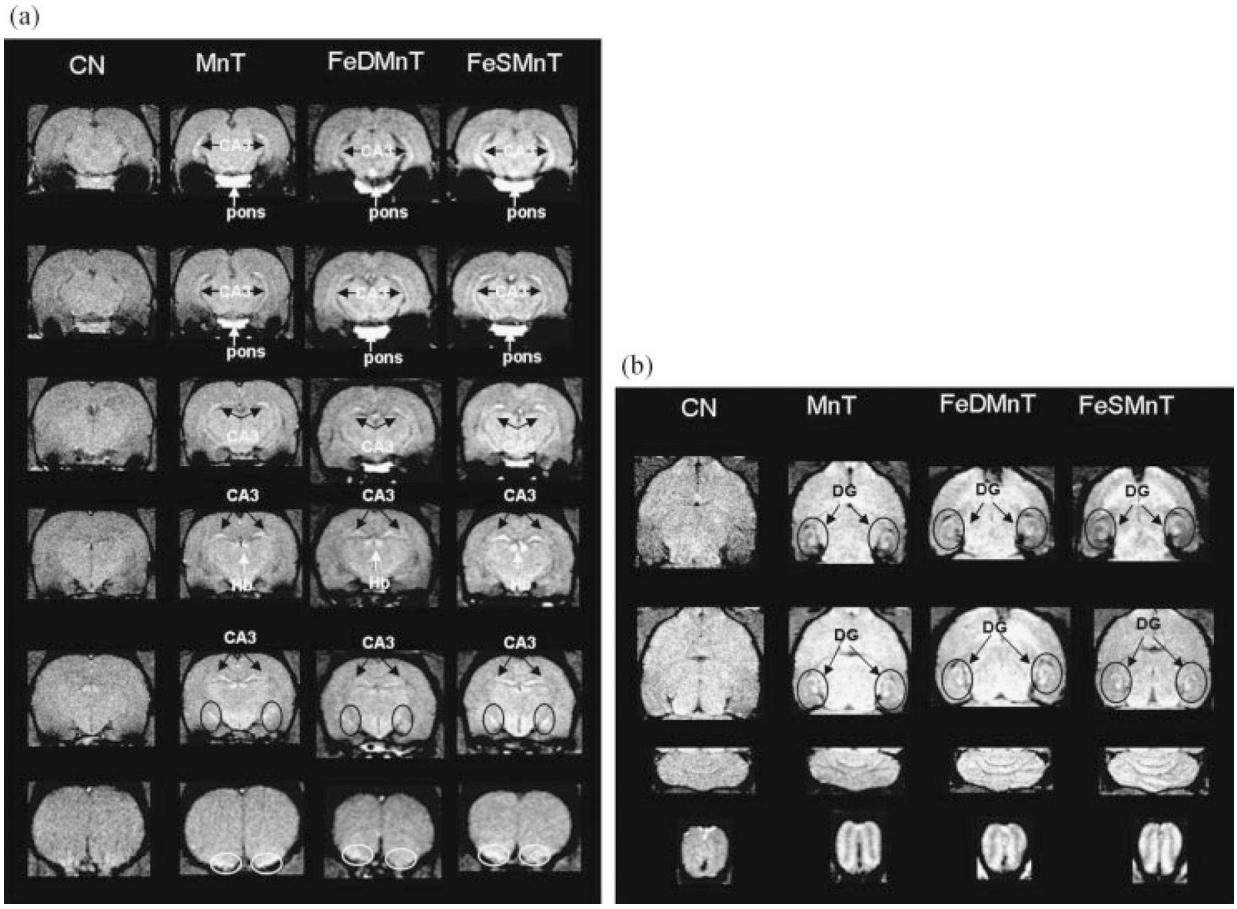

Figure 1.

T1 weighted images for rats in CN (1st column in a and b), MnT (2nd column in a and b), FeDMnT (3rd column in a and b) and FeSMnT (4th column in a and b) groups at week 14 (TR=500 ms, flip angle=70). (a) Transverse direction. (b) Coronal direction. CB, cerebellum; BS, brainstem; MB, midbrain; HP, hippocampus; ST, striatum; CX, cortex.

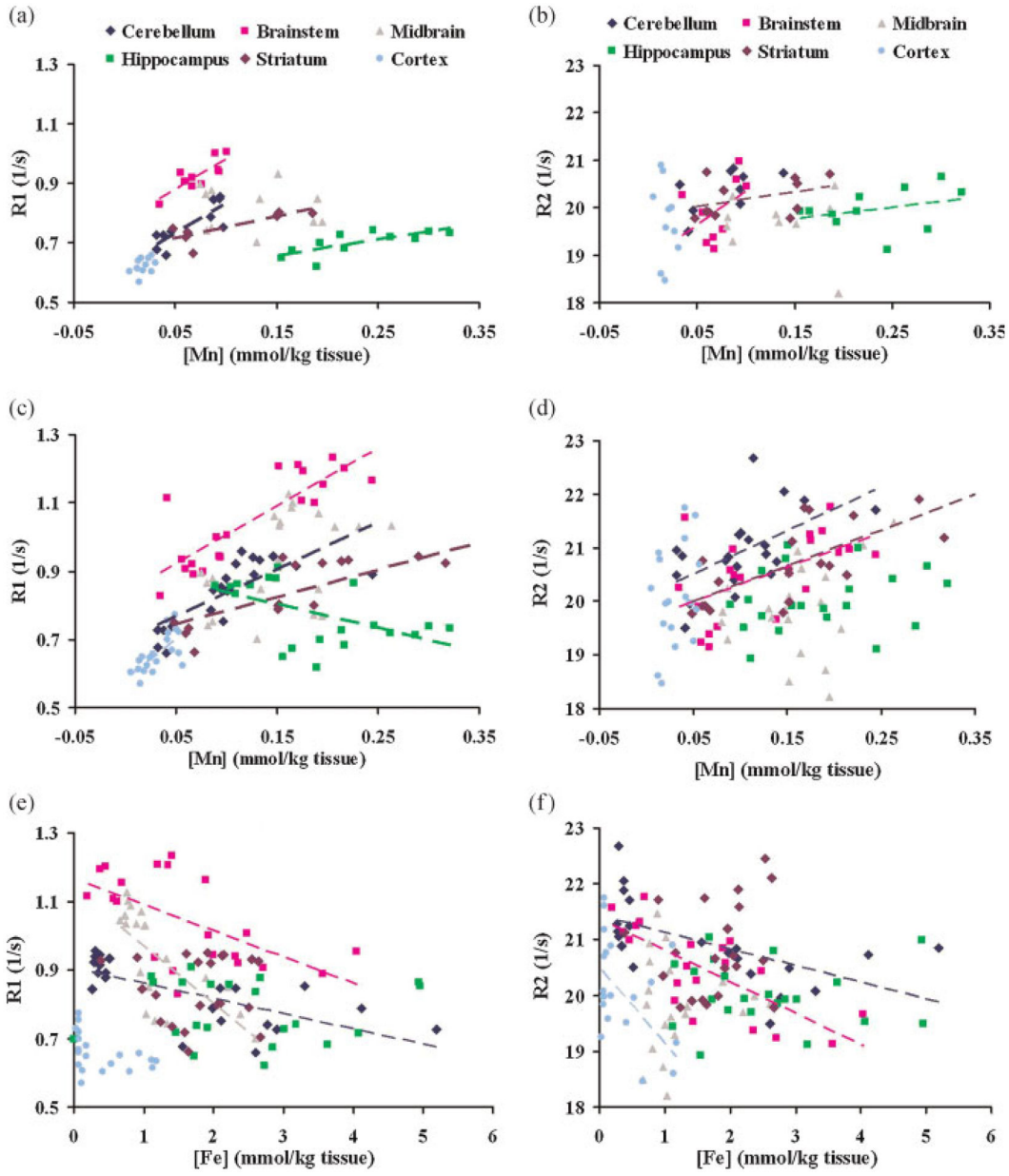

Figure 2.

Fitting results of simple linear model using eqn (1). (a) R1 *versus* [Mn] when only CN and MnT groups are considered. (b) R2 *versus* [Mn] when only CN and MnT groups are considered. (c) R1 *versus* [Mn] when all four groups (CN, MnT, FeDMnT, FeSMnT) are considered. (d) R2 *versus* [Mn] when all four groups (CN, MnT, FeDMnT, FeSMnT) are considered. (e) R1 *versus* [Fe] when all four groups (CN, MnT, FeDMnT, FeSMnT) are considered. (f) R2 *versus* [Fe] when all four groups (CN, MnT, FeDMnT, FeSMnT) are considered.

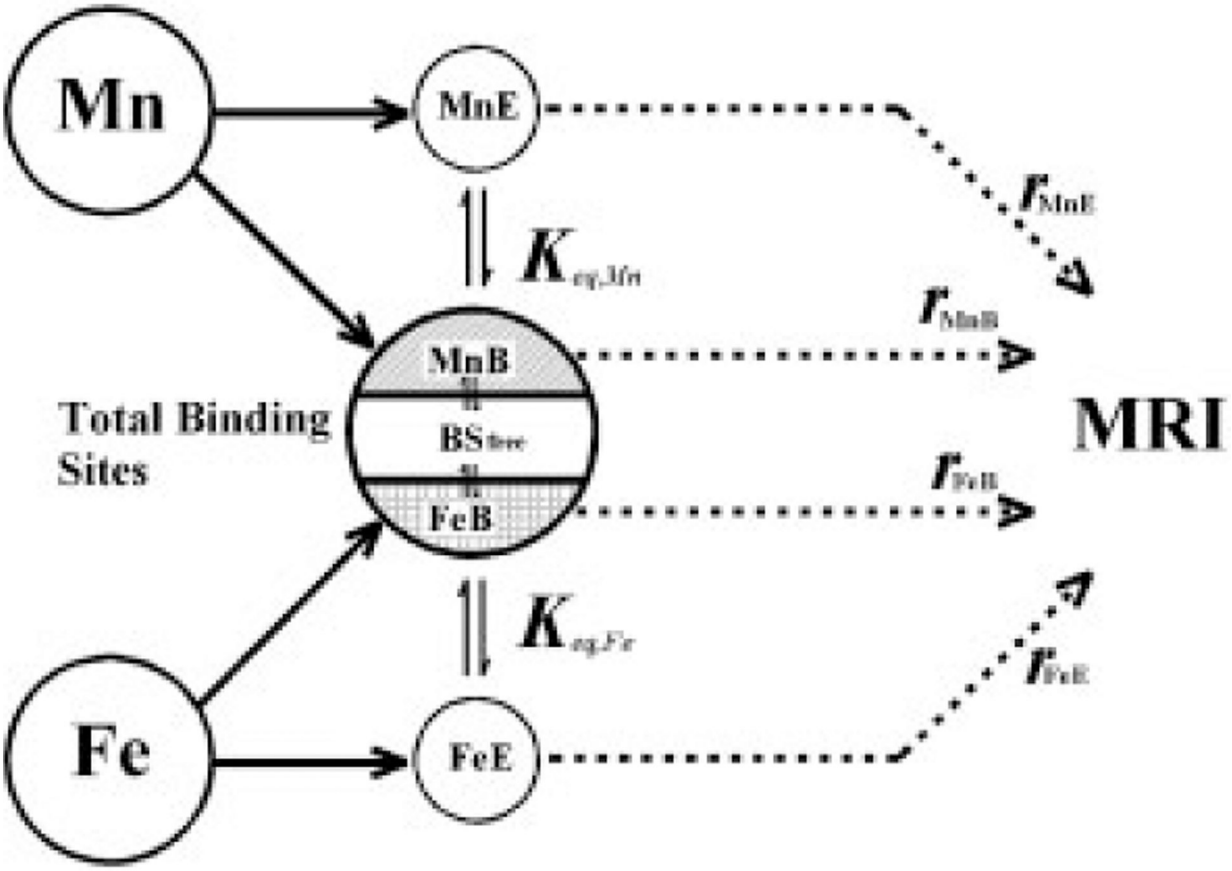

Figure 3.
Principles of the competition model.

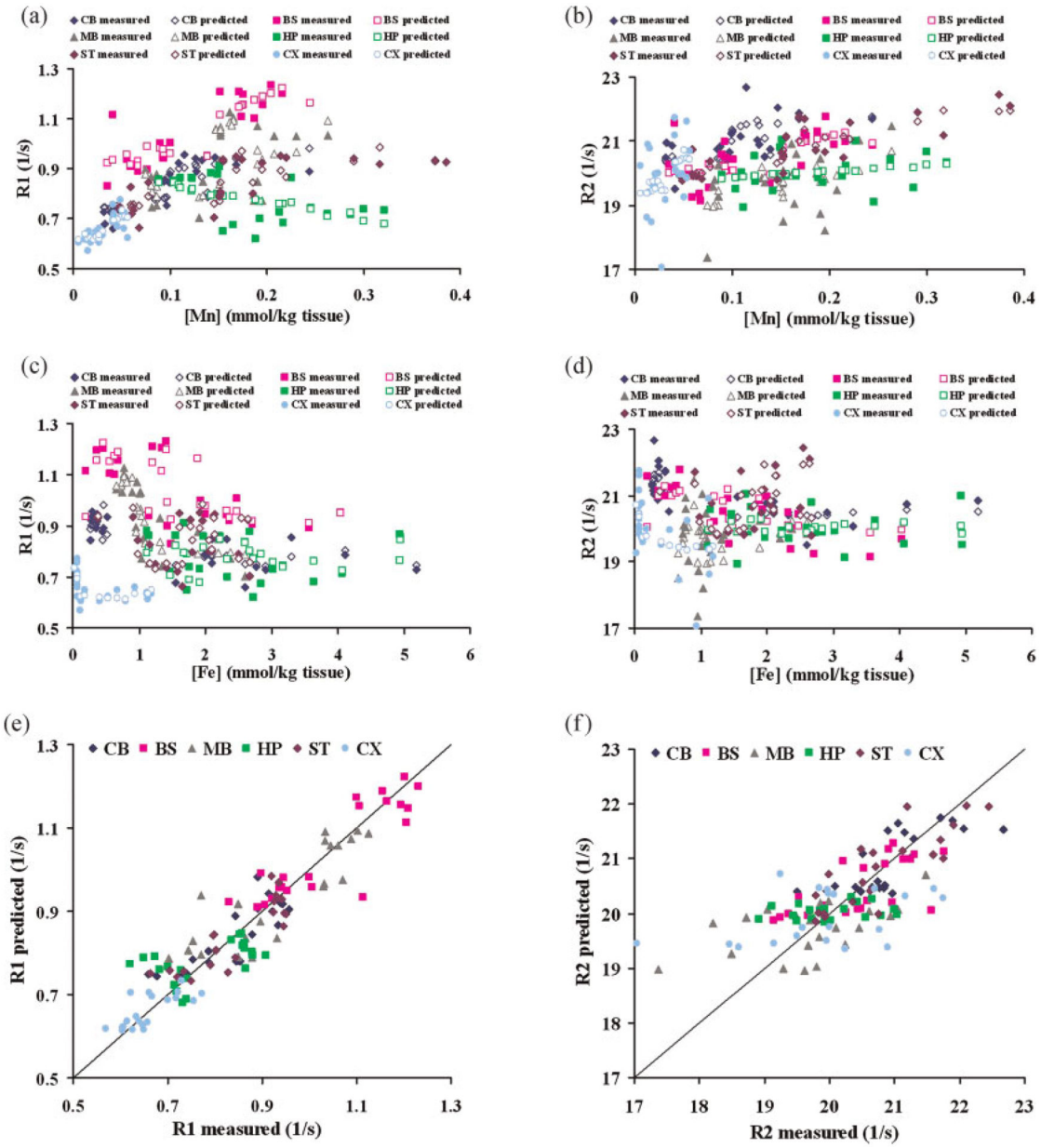

Figure 4.

Fitting results of the competition model. (a) Measured and predicted R1 values *versus* Mn concentration at six brain regions. Solid symbols for measured values, hollow symbols for predicted values. (b) Measured and predicted R_2 values *versus* Mn concentration at six brain regions. Solid symbols for measured values, hollow symbols for predicted values. (c) Measured and predicted R_1 values versus Fe concentration at six brain regions. Solid symbols for measured values, hollow symbols for predicted values. (d) Measured and predicted R_2 values *versus* Fe concentration at six brain regions. Solid symbols for measured values, hollow symbols for predicted values. (e) Predicted R_1 values *versus* measured R_1 values at six brain regions. (f) Predicted R_2 values *versus* measured R_2 values at six brain

regions. CB, cerebellum; BS, brainstem; MB, midbrain; HP, hippocampus; ST, striatum; CX, cortex.

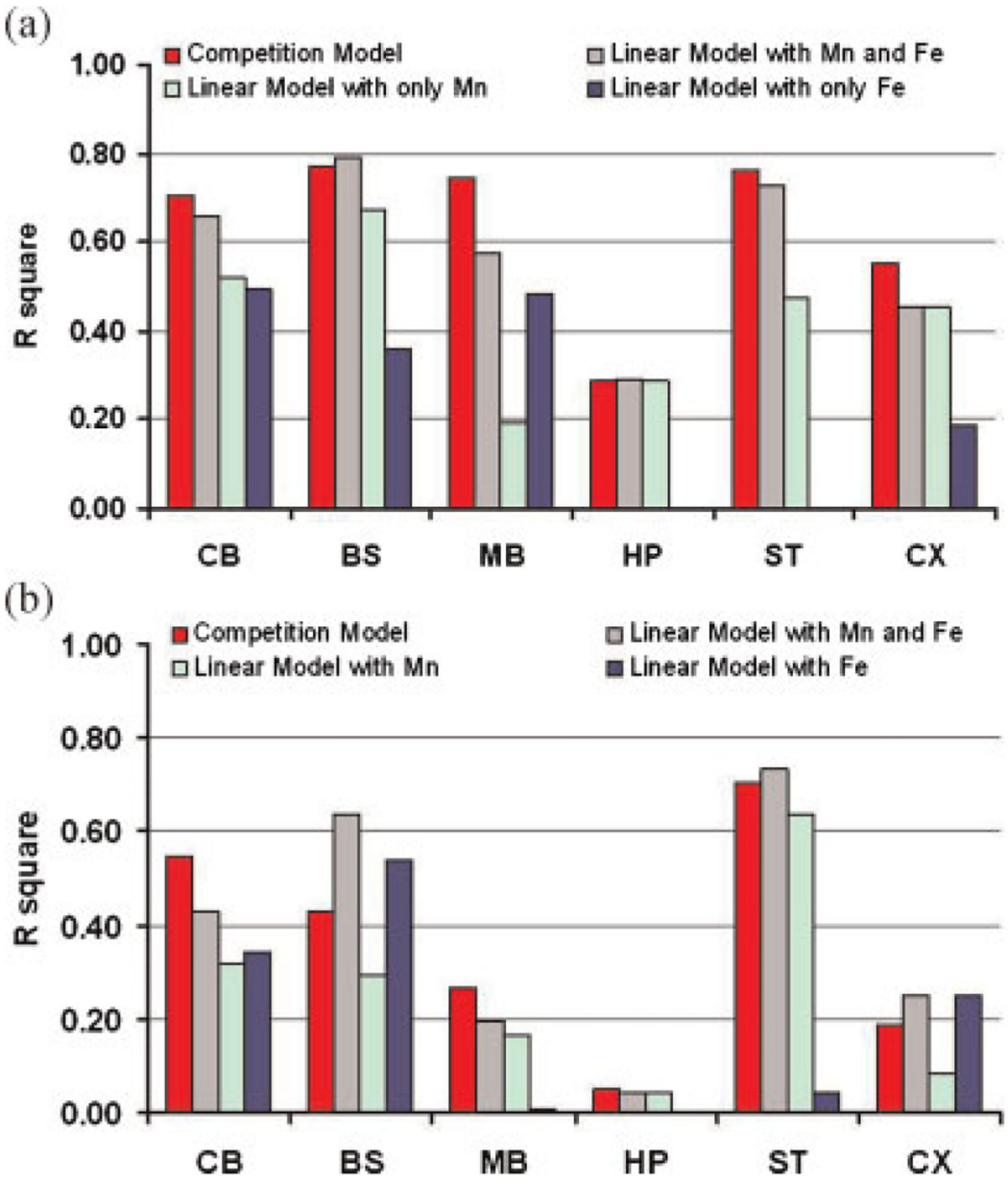

Figure 5.

Square of the correlation coefficient between the measured relaxation rate and the predicted relaxation rate derived by competition and linear models. (a) r^2 of measured R_1 *versus* fitted R_1 as results of using competition and linear models. (b) r^2 of measured R_2 *versus* fitted R_2 as results of using competition and linear models. CB, cerebellum; BS, brainstem; MB, midbrain; HP, hippocampus; ST, striatum; CX, cortex.

Table 1.

Metal concentrations measured by GFAAS at the 14th week

	CN	MnT	FeDMnT	FeSMnT
(a) Mn concentrations (10^{-2} mmolMn/kg wet weight) measured by GFAAS at the 14th week				
CB	3.8±0.26^{a,b,c}	9.9±0.81^{a}	13.8±2.20^{c}	13.5±1.40^{b}
BS	5.7±0.59^{a,b,c}	9.9±0.86^{a,e}	17.3±2.92^{c}	18.2±0.79^{b,e}
MB	13.6±2.40	12.0±1.91	18.3±1.32	18.5±2.66
HP	18.4±1.08^{a,c}	27.2±1.60^{a,e,f}	11.9±0.56^{c,f}	15.4±2.80^{e}
ST	7.7±1.75^{c}	13.0±2.03	22.3±2.69^{c}	28.9±5.37
CX	1.9±0.31^{b,c}	2.0±0.36^{e,f}	4.9±0.21^{c,f}	4.5±0.34^{b,e}
(b) Fe concentrations (mmol Fe/kg wet weight) measured by GFAAS at the 14th week				
CB	3.01±0.60^{b,c}	2.65±0.35^{e,f}	0.39±0.04^{c,f}	0.33±0.02^{b,e}
BS	2.25±0.43^{c}	2.36±0.37^{e,f}	0.87±0.26^{c,f}	0.89±0.25^{e}
MB	1.70±0.33	1.42±0.21	0.87±0.06	0.79±0.04
HP	2.19±0.63	2.57±0.41	2.22±0.59	2.88±0.72
ST	1.7±0.25	1.77±0.24	1.63±0.26	2.06±0.40
CX	0.64±0.23	0.66±0.14^{e,f}	0.06±0.01^{f}	0.10±0.03^{e}

Note: CB, cerebellum; BS, brainstem; MB, midbrain; HP, hippocampus; ST, striatum; CX, cortex.

The data represent mean values±standard error averaged across animals a–f represents statistical difference at $p<0.05$.

^{a}CN *versus* MnT;

^{b}CN *versus* FeSMnT;

^{c}CN *versus* FeDMnT;

^{d}FeSMnT *versus* FeDMnT;

^{e}MnT *versus* FeSMnT;

^{f}MnT *versus* FeDMnT.

Table 2.

Relaxation rates measured by MRI at the 14th week

	CN	MnT	FeDMnT	FeSMnT
(a) Longitudinal relaxation rate R_1 (10^{-1} s^{-1}) measured by MRI at the 14th week				
CB	7.06±0.16^{a,b,c}	8.12±0.17^{a,e,f}	8.96±0.18^{c,f}	9.34±0.08^{b,e}
BS	8.96±0.19^{b,c}	9.57±0.16^{e,f}	11.57±0.22^{c,f}	11.85±0.23^{b,e}
MB	7.48±0.13^{a,b,c}	8.78±0.13^{a,e,f}	10.49±0.12^{c,f}	10.80±0.17^{b,e}
HP	6.64±0.14^{a,b,c}	7.29±0.04^{a,e,f}	8.59±0.07^{c,f}	8.77±0.09^{b,e}
ST	7.14±0.15^{a,b,c}	8.10±0.08^{a,e,f}	9.36±0.07^{c,f}	9.34±0.03^{b,e}
CX	6.19±0.14^{b,c}	6.25±0.09^{e,f}	7.05±0.26^{c,f}	6.99±0.17^{b,e}
(b) Transverse relaxation rate R_2 (s^{-1}) measured by MRI at the 14th week				
CB	20.35±0.28^{b}	20.58±0.12^{e}	21.11±0.17	21.94±0.31^{b,e}
BS	19.59±0.21^{b,c}	20.24±0.25^{f}	21.17±0.19^{c,f}	20.88±0.23^{b}
MB	19.43±0.33	19.51±0.45	19.48±0.39	20.72±0.34
HP	19.93±0.08	20.00±0.24	19.70±0.23^{d}	20.69±0.26^{d}
ST	19.85±0.03^{a,b,c}	20.49±0.12^{a,e}	21.19±0.23^{c}	21.97±0.20^{b,e}
CX	19.77±0.47	19.23±0.50^{e}	19.97±0.19	21.35±0.20^{e}

Note: CB, cerebellum; BS, brainstem; MB, midbrain; HP, hippocampus; ST, striatum; CX, cortex.

The data represent mean values±standard error averaged across animals a–f represents statistical difference at $p<0.05$.

^{a}CN *versus* MnT;

^{b}CN *versus* FeSMnT;

^{c}CN *versus* FeDMnT;

^{d}FeSMnT *versus* FeDMnT;

^{e}MnT *versus* FeSMnT;

^{f}MnT *versus* FeDMnT.

Table 3.

Relaxivities of Mn (s/mM) in rat brain regions – fitting results of eqn 1 applied only to CN and MnT groups, compared with relaxivities (s/mM) for $MnCl_2$ phantoms

	Phantom	CB	BS	MB	HP	ST	CX
(a) r_1 value, (mean±standard error), significance of r_1 and r^2							
r_1	8.39±0.28	1.62±0.39	1.65±0.40	−0.14±0.41	0.42±0.13	0.58±0.17	1.08±0.84
p	2.470E−10	0.003	0.003	0.743	0.009	0.016	0.233
r^2	0.99	0.69	0.68	0.01	0.55	0.65	0.15
(b) r_2 value, (mean±standard error), significance of r_2 and r^2							
r_2	145.82±3.88	6.11±3.27	11.56±8.45	2.67±4.95	1.98±1.97	2.48±1.90	−49.11±35.69
p	3.350E−11	0.104	0.214	0.593	0.340	0.224	0.202
r^2	0.99	0.33	0.21	0.03	0.10	0.16	0.17
(c) Summarized r_1, r_2, and r_2/r_1,							
r_1	8.39	1.62	1.65	−0.14	0.42	0.58	1.08
r_2	145.82	6.11	11.56	2.67	1.98	2.48	−49.11
r_2/r_1	17.38	3.77	7.00	−19.07	4.71	4.28	−45.47

Note: CB, cerebellum; BS, brainstem; MB, midbrain; HP, hippocampus; ST, striatum; CX, cortex.

The data represent mean values±standard error.

The relaxivities of brain tissues are changed to units of (s/mM) by assuming 80% water content in brain tissues.

p – significance of the relaxivities.

r^2 – square of correlation coefficient.

Table 4.

Results of least squares fitting to eqn (1) when all four groups of rats are considered. Relaxation rates were fitted against Mn Fe concentrations separately

	$r_{1,Mn}$	p	r^2_{Mn}
(a) r_1 of Mn (Mean±SE), significance of $r_{1,Mn}$ and square of correlation coefficient			
CB	1.31±0.29	2.15E−04	0.52
BS	1.66±0.27	5.62E−06	0.67
MB	1.16±0.54	4.59E−02	0.19
HP	−0.7±0.25	1.22E−02	0.29
ST	0.65±0.16	5.67E−04	0.47
CX	2.34±0.60	1.12E−03	0.45
	$r_{1,Fe}$	p	r^2_{Fe}
(b) r_1 of Fe (MeaniSE), significance of $r_{1,fe}$ and square of correlation coefficient			
CB	−0.04±0.01	3.95E−04	0.49
BS	−0.08±0.02	4.00E−03	0.36
MB	−0.17±0.04	4.45E−04	0.49
HP	−0.00±0.02	9.81 E−01	0.00
ST	0.00±0.04	9.34E−01	0.00
CX	−0.06±0.03	5.52E−02	0.19
	$r_{2,Mn}$	p	r^2_{Mn}
(c) r_2 of Mn (Mean±SE), significance of $r_{2,Mn}$ and square of correlation coefficient			
CB	8.10±2.72	7.69E−03	0.32
BS	6.45±2.31	1.17E−02	0.29
MB	7.65±3.97	6.90E−02	0.16
HP	1.75±1.88	3.65E−01	0.04
ST	6.64±1.15	1.45E−05	0.64
CX	20.02±15.62	2.16E−01	0.08
	$r_{2,Fe}$	p	r^2_{Fe}
(d) r_2 of Fe (Mean±SE), significance of $r_{2,Fe}$ and square of correlation coefficient			
CB	−0.29±0.09	5.26E−03	0.34
BS	−0.55±0.12	1.50E−04	0.55
MB	0.14±0.39	7.21 E−01	0.007
HP	−0.02±0.12	8.60E−01	0.002
ST	0.28±0.31	3.76E−01	0.042
CX	−1.31±0.54	2.55E−02	0.26

Note: CB, cerebellum; BS, brainstem; MB, midbrain; HP, hippocampus; ST, striatum; CX, cortex.

Unit of r_1 and r_2 is [s mmol/kg tissue]$^{-1}$.

p – significance of the relaxivities.

r^2 – square of correlation coefficient.

Table 5.

Results of least squares fitting to eqns (2) and (3) assuming relaxation rates are linear combination of contributions of Mn and Fe, which exist independently in the brain

	$r_{1,Mn}$	$r_{1,Fe}$	p_{Mn}	p_{Fe}	r^2
(a) r_1 (Mean±SE), significances of r_1 and square of correlation coefficient					
CB	0.88±0.30	−0.028±0.010	8.38E−03	1.54E−02	0.66
BS	1.41±0.23	−0.047±0.015	9.82E−06	4.99E−03	0.79
MB	0.80±0.42	−0.15±0.038	7.07E−02	8.34E−04	0.57
HP	−0.71±0.26	0.004±0.015	1.42E−02	7.85E−01	0.29
ST	0.99±0.14	−0.096±0.024	1.86E−06	7.06E−04	0.73
CX	2.36±0.82	0.001±0.031	1.06E−02	9.63E−01	0.45
	$r_{2,Mn}$	$r_{2,Fe}$	p_{Mn}	p_{Fe}	r^2
(b) r_2 (Mean±SE), significances of r_2 and square of correlation coefficient					
CB	5.02±3.04	−0.20±0.11	1.16E−01	7.75E−02	0.43
BS	3.94±1.81	−0.48±0.11	4.28E−02	6.28E−04	0.65
MB	8.38±4.10	0.31±0.37	5.57E−02	4.20E−01	0.19
HP	1.75±1.94	−0.00±0.11	3.79E−01	9.71 E 01	0.04
ST	8.44±1.24	−0.52±0.20	2.23E−06	2.11E−02	0.73
CX	−4.49±19.24	−1.42±0.73	8.18E−01	6.86E−02	0.25

Note: CB, cerebellum; BS, brainstem; MB, midbrain; HP, hippocampus; ST, striatum; CX, cortex.

p – significance of the relaxivities.

r^2 – square of correlation coefficient.

Table 6.

Results of competition model

	CB	BS	MB	HP	ST	CX
(a) Longitudinal relaxivities for MnB, MnE, FeB and FeE in different brain regions						
$r_{1,MnB}$**	1.74±0.24	1.65±0.20	2.75±0.29	0.25±0.32	1.92±0.25	7.65±1.16
$r_{1,MnE}$**	0.54±0.30	0.34±0.46	Null	Null	Null	Null
$r_{1,FeB}$**	Null	Null	0.36±0.17	1.15±0.33	Null	0.07±0.03
$r_{1,FeE}$**	Null	Null	Null	Null	Null	0.06±0.02
(b) Transverse relaxivities for MnB, MnE, FeB, and FeE in different brain regions						
$r_{2,MnB}$**	15.49±2.41	7.01±1.70	21.96±3.57	3.57±2.38	12.03±2.40	63.52±31.32
$r_{2,MnE}$**	0.75±3.0	Null	3.37±3.62	Null	3.83±1.47	Null
$r_{2,FeB}$**	2.16±1.92	Null	7.13±2.10	1.16±2.42	Null	Null
$r_{2,FeE}$**	0.05±0.08	Null	0.86±0.38	Null	Null	Null

Note: CB, cerebellum; BS, brainstem; MB, midbrain; HP, hippocampus; ST, striatum; CX, cortex.

The data represent mean values±standard error averaged across animals.

** unit: [s mmol/kg tissue]$^{-1}$.

Table 7.

Predicted MnB, MnE, FeB, FeE concentrations for CN, MnT, FeSMnT and FeDMnT groups

	CB	BS	MB	HP	ST	CX
(a) Averaged MnB, MnE, FeB, FeE and BS_{free} concentrations (10^{-1} mmol/kg tissue) for control group						
MnB	0.025±0.004	0.32±0.07	0.25±0.12	1.62±0.07	0.54±0.02	0.04±0.01
MnE	0.35±0.03	0.25±0.10	1.10±0.21	0.22±0.04	0.23±0.16	0.15±0.03
FeB	4.126±0.005	15.94±1.25	9.37±0.12	2.20±0.07	13.96±0.53	0.25±0.02
FeE	25.94±5.95	6.60±3.31	7.63±3.19	24.33±3.19	3.13±2.13	6.16±2.29
BS_{free}	0.003±0.001	1.79±1.19	0.02±0.01	0.024±0.004	1.32±0.54	0.010±0.004
(b) Averaged MnB, MnE, FeB, FeE and BS_{free} concentrations (10^{-1} mmol/kg tissue) for MnT group						
MnB	0.067±0.005	0.54±0.07	0.30±0.09	2.30±0.13	0.82±0.08	0.03±0.01
MnE	0.93±0.08	0.45±0.15	0.90±0.17	0.42±0.06	0.48±0.15	0.17±0.03
FeB	4.083±0.005	16.95±0.56	9.30±0.10	1.53±0.13	13.31±0.92	0.26±0.01
FeE	22.44±3.52	6.68±3.36	4.91±1.98	24.15±4.05	4.36±1.57	6.38±1.44
BS_{free}	0.003±0	0.56±0.51	0.05±0.02	0.017±0.002	1.69±0.96	0.005±0.002
(c) Averaged MnB, MnE, FeB, FeE and BS_{free} concentrations (10^{-1} mmol/kg tissue) for FeSMnT group						
MnB	1.02±0.02	1.80±0.07	1.39±0.02	1.34±0.19	1.45±0.11	0.16±0.01
MnE	0.33±0.13	0.02±0.01	0.45±0.28	0.20±0.10	1.44±0.55	0.29±0.02
FeB	2.92±0.08	8.82±2.47	7.63±0.20	2.47±0.19	12.97±1.35	0.11±0.01
FeE	0.37±0.15	0.03±0.02	0.24±0.16	26.29±7.30	7.60±2.73	0.58±0.02
BS_{free}	0.22±0.09	7.43±2.51	0.62±0.20	0.03±0.01	1.39±1.27	0.018±0.001
(d) Averaged MnB, MnE, FeB, FeE and BS_{free} concentrations (10^{-1} mmol/kg tissue) for FeDMnT group						
MnB	0.87±0.09	1.59±0.25	1.11±0.12	1.10±0.07	1.45±0.08	0.18±0.01
MnE	0.51±0.20	0.14±0.13	0.72±0.25	0.09±0.02	0.78±0.22	0.31±0.02
FeB	3.10±0.15	8.23±2.24	8.03±0.37	2.69±0.08	12.38±1.72	0.10±0.01
FeE	0.79±0.28	0.43±0.42	0.66±0.26	19.55±5.85	3.89±1.04	0.50±0.07
BS_{free}	0.18±0.09	8.23±2.32	0.52±0.26	0.05±0.01	1.99±1.70	0.019±0.002

Note: CB, cerebellum; BS, brainstem; MB, midbrain; HP, hippocampus; ST, striatum; CX, cortex.

The data represent mean values±standard error averaged across animals.

Table 8.

Comparison of the fitting results between the competition or linear models (correlation coefficient, 95% confidence interval of the correlation coefficient as well as the *p* values)

	CB	BS	MB	HP	ST	CX
(a) Fitting results of R_1						
(1) Competition model						
CC	0.84	0.88	0.86	0.54	0.87	0.74
95% CI	[0.64, 0.93]	[0.72, 0.95]	[0.69, 0.94]	[0.13, 0.79]	[0.71, 0.95]	[0.45, 0.89]
p	1.96E−06	1.81E−07	5.06E−07	1.24E−02	2.49E−07	1.73E−04
(2) Linear model with both Mn and Fe considered						
CC	0.81	0.89	0.76	0.54	0.85	0.67
95% CI	[0.58, 0.92]	[0.74, 0.95]	[0.48, 0.90]	[0.14, 0.79]	[0.67, 0.94]	[0.33, 0.86]
p	8.06E−06	7.29E−08	7.06E−05	1.17E−02	9.48E−07	1.12E−03
(3) Linear model with only Mn is considered						
CC	0.72	0.82	0.44	0.54	0.69	0.67
95% CI	[0.42, 0.88]	[0.60, 0.92]	[0.01, 0.73]	[0.14, 0.79]	[0.36, 0.86]	[0.33, 0.86]
p	2.15E−04	5.62E−06	4.59E−02	1.22E−02	5.67E−04	1.12E−03
(4) Linear model with only Fe is considered						
CC	0.70	0.60	0.70	0.01	0.02	0.44
95% CI	[0.39, 0.87]	[0.23, 0.82]	[0.38, 0.87]	[−0.43, 0.44]	[−0.42, 0.45]	[−0.01, 0.74]
p	3.95E−04	4.00E−03	4.45E−04	9.81 E—01	9.34E−01	5.52E−02
(b) Fitting results of R_2						
(1) Competition model						
CC	0.74	0.65	0.52	0.23	0.84	0.43
95% CI	[0.45, 0.89]	[0.31, 0.85]	[0.11, 0.78]	[−0.23, 0.60]	[0.64, 0.93]	[−0.01,0.73]
p	1.28E−04	1.28E−03	1.65E−02	3.19E−01	2.07E−06	5.78E−02
(2) Linear model with both Mn and Fe considered						
CC	0.66	0.80	0.44	0.21	0.86	0.50
95% CI	[0.31, 0.85]	[0.56, 0.91]	[0.01, 0.73]	[−0.24, 0.59]	[0.67, 0.94]	[0.07, 0.77]
p	1.26E−03	1.51E−05	4.56E−02	3.59E−01	7.61 E−07	2.47E−02
(3) Linear model with only Mn is considered						

	CB	BS	MB	HP	ST	CX
CC	0.56	0.54	0.40	0.21	0.80	0.29
95% CI	[0.18, 0.80]	[0.14, 0.79]	[−0.03, 0.71]	[−0.25, 0.59]	[0.56, 0.91]	[−0.18, 0.65]
p	7.69E−03	1.17E−02	6.90E−02	3.65E−01	1.45E−05	2.16E−01
(4) Linear model with only Fe is considered						
CC	0.59	0.73	0.08	0.04	0.20	0.50
95% CI	[0.21, 0.81]	[0.44, 0.89]	[−0.36, 0.50]	[−0.40, 0.46]	[−0.25, 0.58]	[0.07, 0.77]
p	5.26E−03	1.50E−04	7.21 E−01	8.60E−01	3.76E−01	2.55E−02

Note: CB, cerebellum; BS, brainstem; MB, midbrain; HP, hippocampus; ST, striatum; CX, cortex.